Materials and Design 55 (2014) 176–182

Contents lists available at ScienceDirect

Materials and Design

journal homepage: www.elsevier.com/locate/matdes

Characterization of friction stir welded boron carbide particulate reinforced AA6061 aluminum alloy stir cast composite

K. Kalaiselvan [a,*], I. Dinaharan [b], N. Murugan [c]

[a] Department of Mechanical Engineering, K.S. Rangasamy College of Technology, Tiruchengode 637 215, Tamil Nadu, India
[b] Department of Mechanical Engineering, V V College of Engineering, Tisaiyanvilai 627 657, Tamil Nadu, India
[c] Department of Mechanical Engineering, Coimbatore Institute of Technology, Coimbatore 641 014, Tamil Nadu, India

ARTICLE INFO

Article history:
Received 18 May 2013
Accepted 28 September 2013
Available online 8 October 2013

Keywords:
A. Non-ferrous metals and alloys
D. Welding
E. Mechanical properties
F. Microstructure

ABSTRACT

Development of welding procedures to join aluminum matrix composite (AMCs) holds the key to replace conventional aluminum alloys in many applications. In this research work, AA6061/B_4C AMC was produced using stir casting route with the aid of K_2TiF_6 flux. Plates of 6 mm thickness were prepared from the castings and successfully butt joined using friction stir welding (FSW). The FSW was carried out using a tool rotational speed of 1000 rpm, welding speed of 80 mm/min and axial force of 10 kN. A tool made of high carbon high chromium steel with square pin profile was used. The microstructure of the welded joint was characterized using optical and scanning electron microscopy. The welded joint showed the presence of four zones typically observed in FSW of aluminum alloys. The weld zone showed fine grains and homogeneous distribution of B_4C particles. A joint efficiency of 93.4% was realized under the experimental conditions. But, FSW reduced the ductility of the composite.

1. Introduction

Aluminum matrix composites (AMCs) have captured the attention of the materials community to a large extent. AMCs combine the advantages of aluminum alloys and the special properties of ceramic particles [1]. AMCs possess high specific stiffness, high strength to weight ratio at room or elevated temperatures, excellent fatigue properties, high formability and improved wear resistance [2,3]. AMCs have become a major focus in aircraft, automotive and marine industries due to those excellent properties. But, the replacement of conventional aluminum alloys with AMCs in many applications in the above said industries demands the development of secondary processes such as machining and joining of AMCs [4].

Welding of AMCs using conventional fusion methods degrades the joint properties due to solidification induced structure and chemical reactions [5]. The difference in densities between the matrix and reinforcement materials results in particle segregation. It is difficult to retain the distribution of ceramic particles in the weld zone compared to that of parent composite. The high viscosity of the composite material inhibits material flow which creates a nonuniform distribution of weld stress reducing the joint strength. The heat input during fusion welding often initiates reactions between aluminum matrix and ceramic particles which forms brittle intermetallic compounds in the weld zone. The fusion welded joint is further susceptible to porosity [6–9]. Therefore it is suggested to use solid state welding methods to join AMCs to eliminate those defects. Friction stir welding (FSW) has emerged as a preferred solid state welding method to join AMCs [10].

FSW was invented at The Welding Institute (TWI), UK in 1991. A nonconsumable rotating tool harder than the base material is plunged into the abutting edges of the plates to be joined under sufficient axial force and advanced along the line of the joint. The tool consists of two parts namely shoulder and pin. The material around the tool pin is softened by the frictional heat generated by the tool rotation. Advancement of the tool pushes plastically deformed material from front to back of the tool and forges to complete the joining process [11,12]. Since FSW is a solid state process, a solidification induced structure is absent in the weld zone. Therefore, all the defects related to fusion welding methods are overcome [13].

Some studies on FSW of AMCs reinforced with various ceramic particulates were reported in literatures in recent years [14–23]. Chen et al. [14] studied the microstructure of friction stir welded AA6063/(6, 10.5 vol.%) B_4C and observed substantial grain refinement of aluminum matrix in the weld zone. Vijay and Murugan [15] estimated the effect of various tool pin profiles on microstructural evaluation of friction stir welded AA6061/10 wt.% TiB_2 and reported that the square pin profile yielded higher tensile strength and finer grains in the weld zone. Nami et al. [16] assessed the

* Corresponding author. Tel.: +91 9443952292; fax: +91 04288 274745.
E-mail addresses: kalaiselvanmohit@gmail.com (K. Kalaiselvan), dinaweld2009@gmail.com (I. Dinaharan), murugan@cit.edu.in (N. Murugan).

0261-3069/$ - see front matter © 2013 Elsevier Ltd. All rights reserved.
http://dx.doi.org/10.1016/j.matdes.2013.09.067

Table 1
The chemical composition of AA6061-T6 alloy.

Element	Mg	Si	Fe	Mn	Cu	Cr	Zn	Ni	Ti	Aluminum
wt.%	0.95	0.54	0.22	0.13	0.17	0.09	0.08	0.02	0.01	Balance

effect of tool rotational speed on microstructure of friction stir welded AA6061/15 wt.% Mg_2Si and noticed defects in the weld zone at higher tool rotational speeds. Gopalakrishnan and Murugan [17] developed a mathematical model to predict the tensile strength friction stir welded AA6061/(3–7 wt.%) TiC. Guo et al. [18] applied electron back scattered diffraction technique to precisely reveal the grain size of friction stir welded AA1100/16 vol.% B_4C. Bozkurt et al. [19] evaluated the microstructure of friction stir welded AA2124/25 vol.% SiC in detail and observed cracking of SiC particles and traces of SiO_2 phase in the weld zone. Dinaharan and Murugan [20] analyzed the effect of FSW on microstructure and other properties of AA6061/(0–10 wt.%) ZrB_2 and recorded that FSW shattered the cluster of particles in the parent composite into fine particles of different sizes. Guo et al. [21] noted breakage and fragmentation of particles in friction stir welded AA1100/(16 and 30 vol.%) B_4C. Periyasamy et al. [22] investigated the effect of heat input on microstructure and mechanical properties of friction stir welded AA6061/10 vol.% SiC. Wang et al. [23] obtained enhanced distribution of SiC particles in the weld zone of friction stir welded AA2009/15 vol.% SiC.

The objective of this work is to study the effect of FSW on microstructure and mechanical properties of AA6061/12 wt.% B_4C AMC. The microstructure and properties of as-cast AA6061 are compared with the prepared AMC to comprehend the effect of B_4C particle and FSW. B_4C is a potential reinforcement which has excellent chemical and thermal stability, high hardness and low density and is used for manufacturing of armor tank, neutron shielding material, etc. [24].

2. Experimental procedure

AA6061 rods were melted in an electrical furnace using a coated graphite crucible. The chemical composition and optical photomicrograph of aluminum alloy AA6061-T6 are respectively presented in Table 1 and Fig. 1. The melt was agitated with the help of a mechanical stirrer to form a fine vortex. The mixtures of preheated B_4C particles with an equivalent amount of K_2TiF_6 flux (with 0.1Ti/B_4C ratio) were added at a constant feed rate into the vortex. Argon gas was supplied into the melt during the operation to provide an inert atmosphere. After stirring the molten mixture, it was poured down into the preheated permanent mold. The temperature of the melt was maintained at 860 °C. Castings were taken with various

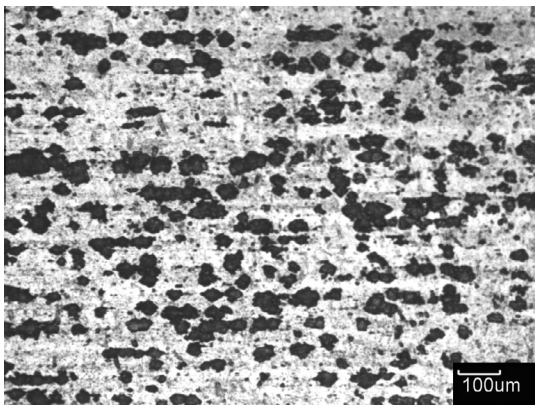

Fig. 1. Optical photomicrograph of as received AA6061-T6 extruded rod.

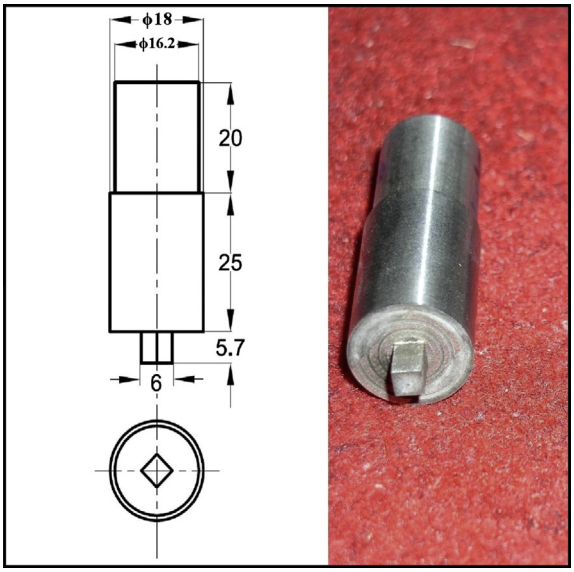

Fig. 2. Dimensions and fabricated friction stir welding tool.

weight percentages (0 and 12 wt.%) of B_4C particles. A detailed fabrication procedure is available elsewhere [25,26].

Plates of size 100 × 50 × 6 mm were prepared from each casting. The butt welding of AA6061/B_4C composites was carried out semi automatically on an indigenously built FSW machine (M/s RV Machine Tools, Coimbatore, INDIA). A tool made of high carbon high chromium steel oil hardened to 62 HRC with square pin profile was used [15]. The dimensions and fabricated tool are shown in Fig. 2. The joints were fabricated at a tool rotational speed of 1000 rpm, welding speed of 80 mm/min and axial force of 10 kN. The parameters were chosen based on several trail runs to produce a defect free weld. Typical FSW defects such as tunnel, pin hole, void, worm hole and piping as shown in Fig. 3 were observed on the trail welded plates.

Specimens were cut from the welded plates to carry out microstructural and mechanical characterization. The specimens were prepared as per standard metallographic procedure and etched with Keller's reagent. The digital image of the macrostructure of the etched specimen was captured using a digital optical scanner. The microstructure was observed using an optical microscope (OLYMPUS-BX51 M) and a scanning electron microscope (JEOL-JSM-6390). X-ray diffraction patterns (XRD) were recorded using Panalytical X-ray diffractometer. The microhardness was measured using a microhardness tester (MITUTOYO-MVK-H1) at 500 g load applied for 15 s. The tensile specimens were prepared as per ASTM: E8M-13a standard having a gauge length of 40 mm, a gauge width of 7 mm and a thickness of 6 mm. The ultimate tensile strength (UTS) was estimated using a computerized universal testing machine (HITECH TUE-C-1000).

3. Results and discussion

3.1. Macrostructure and microstructure of the welded joint

AA6061/B_4C AMC plates of 6 mm thickness were successfully butt welded by FSW. A typical welded plate is shown in Fig. 4.

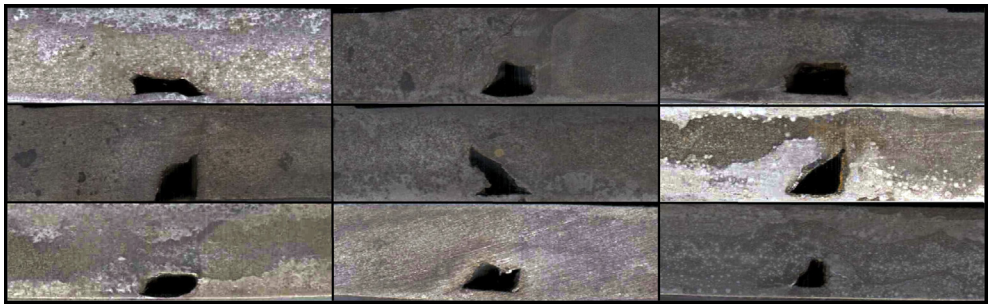

Fig. 3. Typical defects observed in trail welds.

Fig. 4. Friction stir welded plate of AA6061/B_4C AMC.

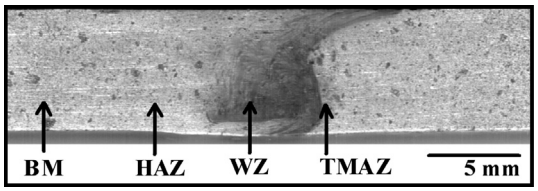

Fig. 5. Macrostructure of the friction stir welded AA6061/B_4C AMC.

The crown surface is characterized by semi circular features which are identical to those formed during the conventional milling process. The rubbing action of the FSW tool shoulder and traversing of tool on the plates to be joined creates such features. This is called as "wake effect" [27]. The crown displays the smooth appearance without the existence of voids, cracks, depressions, discontinuities and excessive flashes. It is important to obtain a proper crown appearance due to the fact that every flaw in the crown leads to some kind of defects in the joint.

The macrostructure of friction stir welded AA6061/B_4C AMC is revealed in Fig. 5. The joint exhibits continuous flow of plasticized material between advancing side and retreating side. Typical FSW defects as shown in Fig. 3 such as tunnels, worm hole and piping are not seen. The frictional heat generated under the selected process parameters is sufficient to exceed the flow stress of the AMC to produce a sound joint. The flow stress of the AMC is relatively higher compared to unreinforced matrix alloy. The flow stress influences the welding window i.e. the range of parameters under which defect free welds can be produced. The presence of B_4C in the AMC offers resistance to the free flow of the matrix alloy during FSW. The welding window of AA6061/B_4C AMC was found to be narrow and several defects were encountered as depicted in Fig. 3. A wider range of parameters could not generate sufficient heat to exceed the flow stress of the AMC. The various zones typically present in FSW of monolithic alloys are visible. The macrostructure consists of parent composite (BM), heat affected zone (HAZ), thermomechanically affected zone (TMAZ) and weld zone (WZ). The various zones are roughly identified by color changes due to the different thermo mechanical histories of the welded AMC. TMAZ is the adjacent zone of weld zone which is affected thermally and experienced plastic deformation. The weld zone on the retreating side is not clearly identified by boundary. Similar observations were reported in the literatures [14,21,28]. The absence of clear boundary at the retreading side can be attributed to the material flow behavior of plasticized composite while forging at the back side of the tool to form the FSP zone.

The SEM micrographs of cast matrix AA6061 and AA6061/B_4C AMC before and after FSW are presented in Fig. 6. The SEM micrograph of as-cast AA6061 depicts (Fig. 6a) dendritic structure of aluminum. The dendritic structure exhibits elongated primary α-Al dendritic arms having a high aspect ratio. The dendritic structure is formed due to high rate of cooling during the solidification of the casting. The secondary precipitation phase Mg_2Si is observed along the dendritic boundaries. The amount of alloying elements including Mg and Si present in AA6061 is higher than the solubility limit. Therefore, intermetallic phases of AA6061 are gathered around the dendritic arms.

The SEM micrograph of AA6061/B_4C AMC reveals (Fig. 6b) the distribution of B_4C particles over the entire matrix alloy. The distribution of B_4C particles is observed fairly homogeneously in the aluminum matrix. Most of the B_4C particles are located in intragranular regions. A cluster of B_4C particles is seen in a few places. It is evident from Fig. 6b that B_4C particles refined the dendritic structure of the as cast matrix alloy. The grain refinement can be attributed to the following two factors: (a) B_4C particles act as nucleation sites for grain formation and (b) aluminum grains solidify on the B_4C particles [29]. The distribution of B_4C particles is the direct result of mechanical stirring and the solidification behavior of the composite melt during casting. Adequate stirring of composite melt during the incorporation of B_4C particles provides good distribution. Suspension of B_4C particles in the aluminum melt is a prerequisite to obtain better distribution. The density gradient between B_4C particle and aluminum is negligible which causing the B_4C particles neither float nor sink in the aluminum melt. The wetting action between molten aluminum and the B_4C particles offers resistance to the free movement of B_4C particles. The above said factors lead to a better distribution of B_4C particles. The velocity of the solidification front influences the B_4C particle to be distributed in intra or inter granular regions [30]. Observing the B_4C particle distribution in the aluminum matrix it appears that the particles are engulfed by the solidification front leading to intra granular regions. There are no voids or porosities around B_4C particles in Fig. 6b. This indicates proper bonding of B_4C

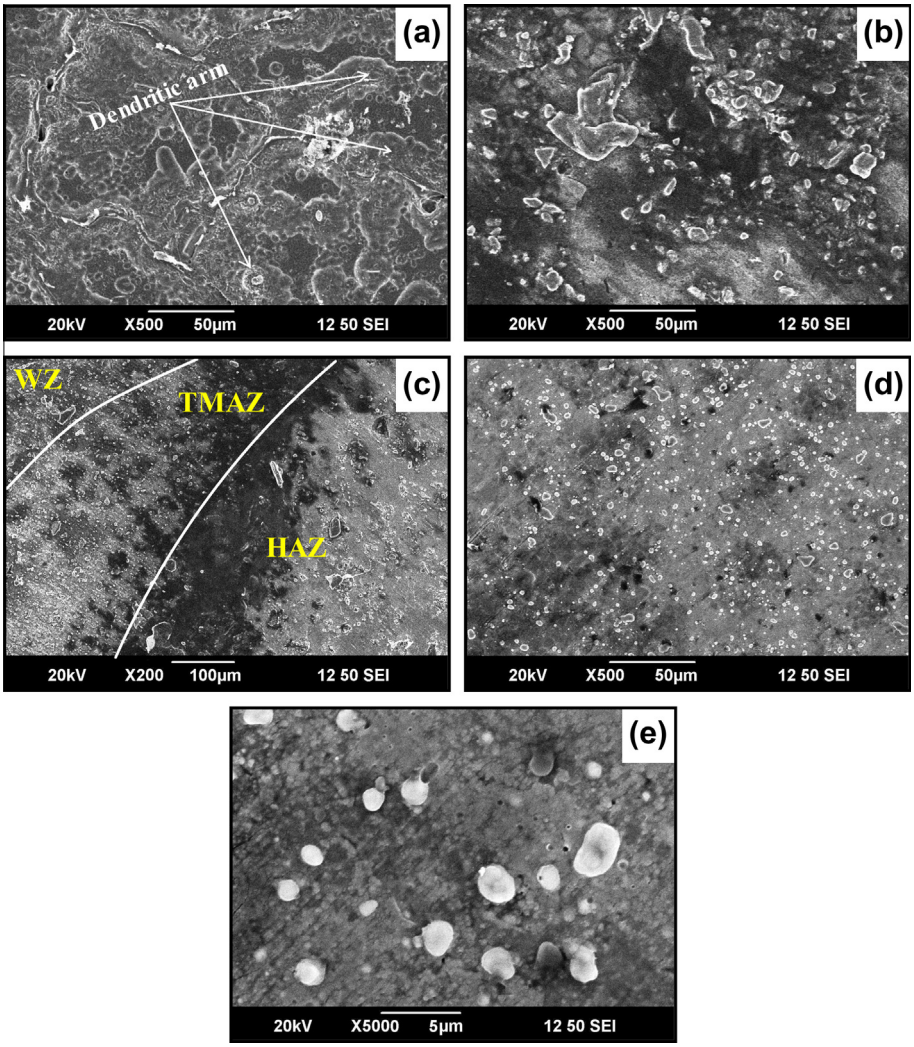

Fig. 6. SEM micrograph of; (a) cast AA6061, (b) cast AA6061/B_4C AMC, (c) transition zone, (d) and (e) weld zone.

particles with the matrix. Stir casting was limited to prepare AA6061/B_4C AMC owing to poor wettability between B_4C particles and the aluminum melt. The addition of K_2TiF_6 flux to the molten matrix enhanced the wettability. The flux facilitates the incorporation of B_4C particles. The flux causes an exothermic reaction in the aluminum melt which evolves heat in the vicinity of B_4C particle–melt interface [31]. The local increase in temperature provides good bonding with the matrix. The XRD pattern of AA6061/B_4C AMC as depicted in Fig. 7 shows the presence of Al and B_4C. No other elements are present in significant quantity. This indicates that B_4C particles did not react with the aluminum matrix to produce any other compounds. The B_4C particles are thermodynamically stable at the synthesizing temperature. The reaction of the particles and the matrix in stir casting sometimes forms undesirable intermetallic phases which will have an adverse effect on the strength of the composite.

The SEM and optical micrograph of the transition zone is presented in Figs. 6c and 8a respectively. Transition zone consists of HAZ and TMAZ. It is difficult to differentiate HAZ and parent composite. The distribution of B_4C particles and grain size are observed to be similar and there is no considerable variation which can be due to the lower thermal sensitivity of the composite. Therefore the transition zone can be considered to be limited to TMAZ in friction stir welded AMCs as reported by others [16,20]. Being exposed to frictional heat, HAZ would have experienced softening. The

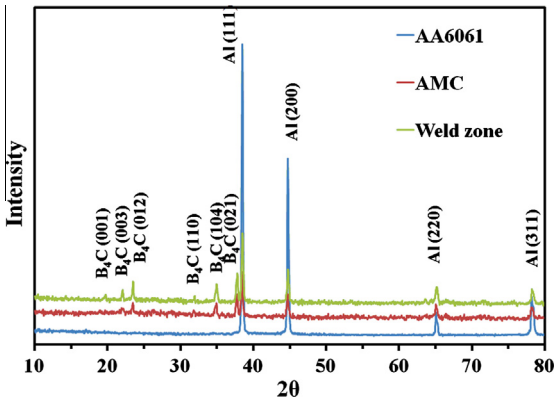

Fig. 7. XRD patterns of AA6061/B_4C AMC before and after FSW.

boundary between the weld zone and TMAZ is clearly visible. TMAZ has elongated and rotated grains (Fig. 8a). TMAZ shows the alignment of B_4C particles in the vertical direction. The distribution of B_4C particles in TMAZ is analogous to parallel bands. TMAZ is subjected to severe plastic deformation due to the frictional heat generated by the rotating tool and the application of stresses. Therefore, B_4C particles are stretched along the shear stress directions.

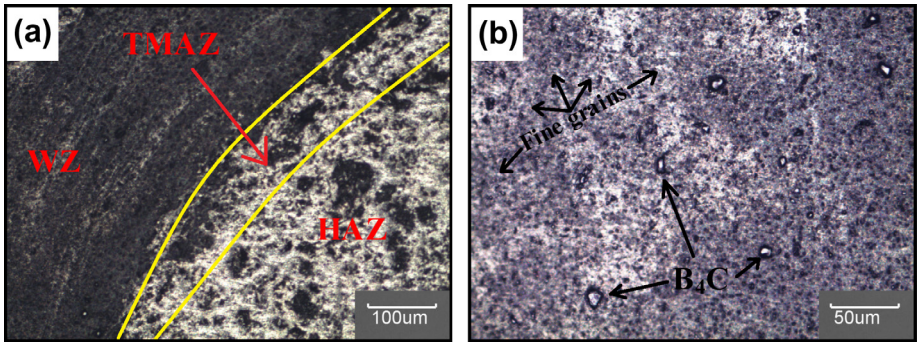

Fig. 8. Optical photomicrographs of; (a) transition zone and (b) weld zone.

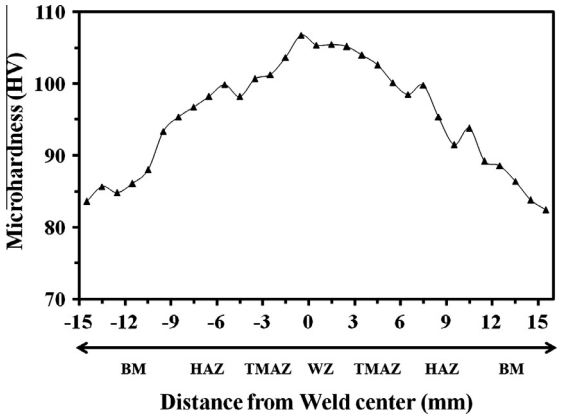

Fig. 9. Microhardness profile across the friction stir welded AA6061/B4C AMC.

The SEM and optical micrograph of weld zone is presented in Figs. 6d and e and 8a respectively. It is clear from those micrographs that the weld zone does not contain porosity or segregation of B_4C particles which are prone in the fusing welding of AMCs. The weld zone is characterized by a homogenous distribution of B_4C particles. The rearrangement of B_4C particles is evident compared to parent composite. The plasticized composite is subjected to the severe strain rate caused by the rotating tool. Therefore, rearrangement of B_4C particles takes place during FSW. The clusters of B_4C particles in the parent composite are shattered into homogeneous distribution. The fine grains in the weld zone (Fig. 8a) indicate dynamic recrystallization during FSW. The XRD pattern of the weld zone (Fig. 7) shows no evidence of any other phase other than the aluminum matrix and B_4C particle. The frictional heat generated during welding did not promote any reaction between the matrix and B_4C particle. Guo et al. [7] observed extensive decomposition of B_4C particles in laser welding AA1100/B_4C AMC. The number of particles in the weld zone appears to be more than the number of particles in the parent composite. It is reflected as a slight increase in the peak of the B_4C particle in the XRD pattern subsequent to FSW. The mechanical stirring action of the tool results in the attrition of bigger size B_4C particles in the parent composite. The debris of fragmented particles will act as nucleation sites leading to grain refinement. The higher magnification micrograph of the weld zone (Fig. 6e) shows the morphology of B_4C particles. There are no sharp corners in the B_4C particles. This can be attributed to the abrasive action of the tool which attempts to round of the particle [32].

3.2. Microhardness of the welded joint

The microhardness profile across the welded joint is presented in Fig. 9. The hardness of weld zone is observed higher to that of parent composite. FSW resulted in an increase in the hardness of AA6061/B_4C AMC. Some investigators recorded hardening of AMCs subsequent to FSW [16,20,22,33]. The hardness of TMAZ and HAZ varied between those of parent composite and weld zone. The band like structure of B_4C particles in the TMAZ contributes to the improvement of hardness. The plasticized composite is exposed to the compressive stresses created by the rotating tool. The compressive stress closes the presence of micro porosities in the cast composite. The dynamic recrystallization during FSW produced finer grains in the weld zone. The fragmentation of bigger B_4C particles gives rise to dislocation density. These factors lead to weld zone hardening.

3.3. Tensile properties of the welded joint

The tensile behavior of AA6061/B_4C AMC before and after FSW is shown in Fig. 10. The reinforcement of B_4C particles increased the ultimate tensile strength (UTS) of the aluminum matrix significantly (Fig. 10a). The mismatch in thermal expansion coefficient

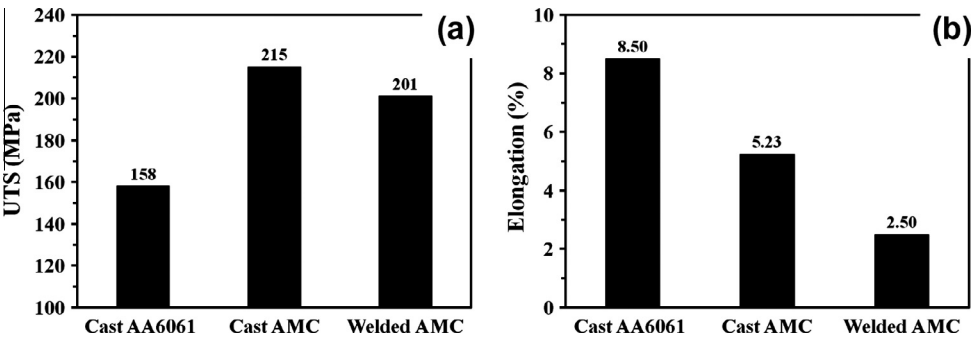

Fig. 10. Tensile behavior of AA6061/B_4C AMC before and after FSW; (a) ultimate tensile strength and (b) elongation.

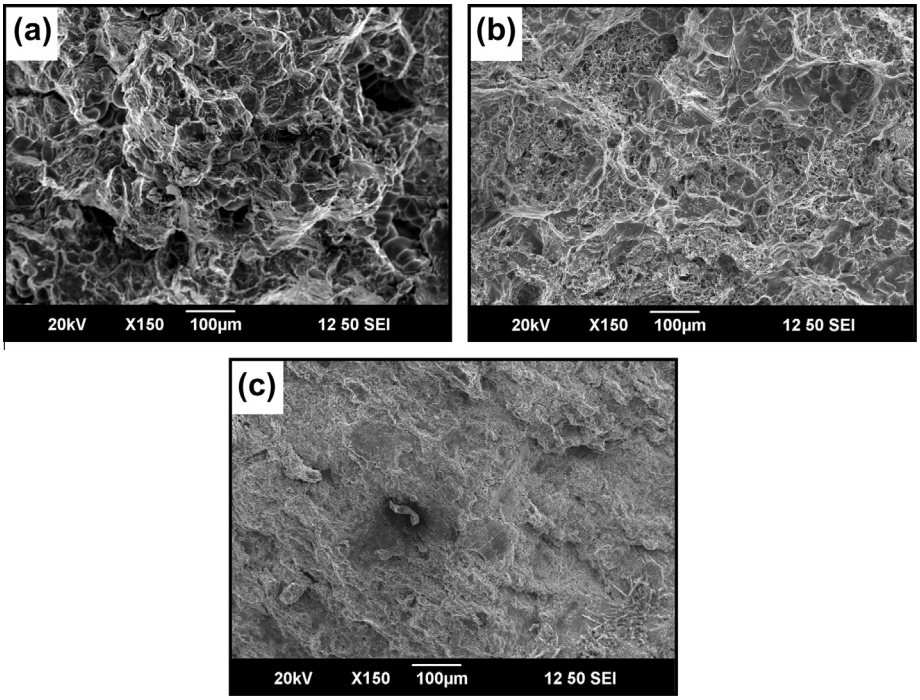

Fig. 11. SEM micrograph of fracture surface of; (a) cast AA6061, (b) cast and (c) welded AA6061/B_4C AMC.

between the matrix and the B_4C particles increases the dislocation density. The interaction between the dislocation and B_4C particles resist the propagation of cracks during tensile loading. The homogeneous distribution of B_4C particles contributes to orowan strengthening. The absence of pores or voids around B_4C particles increases the load bearing capacity of the AMC. Those factors results in the strengthening of the AMC by B_4C particles. It is observed in Fig. 10a that the tensile strength of the friction stir welded AA6061/B_4C AMC is closer to that of parent composite. A joint efficiency of 93.4% was realized under the experimental conditions. The welded joint failed at HAZ. The higher joint efficiency can be attributed to defect free weld zone and proper selection of process parameters. The defects as mentioned in Section 3.1 will act as crack initiation sites and reduce the tensile strength. The combination of process parameters provides good consolidation of material due to optimum stirring, sufficient heat generation and adequate exposure of frictional heat and translation of stirred material. The elongation of welded joint reduced (Fig. 10b) after FSW due to the generation of fine grains and fragmentation of B_4C particles in the weld zone.

The fracture surface of AA6061/B_4C AMC before and after FSW is depicted in Fig. 11. The fracture surface of aluminum matrix depicts (Fig. 11a) a network of large size dimples which confirms large amounts of plastic flow prior to failure. The failure mode is ductile. The fracture surface of AA6061/B_4C AMC shows a network of dimples whose size is smaller compared to the matrix alloy. It indicates a reduction in the ductility of the composite owing to the grain refinement provided by B_4C particles. The fracture surface of friction stir welded AA6061/B_4C AMC does not show a significant number of dimples and the surface is observed to be flat. The amount of plastic flow of the composite during tensile loading is negligible. The failure mode is brittle.

4. Conclusions

The microstructure of friction stir welded AA6061/B_4C AMC was divided into four zones; (i) parent composite, (ii) heat affected zone, (iii) thermomechanically affected zone and (iv) weld zone. It was difficult to differentiate HAZ and parent composite. TMAZ showed a parallel band like distribution of B_4C particles and elongated grains. The weld zone was characterized by a homogenous distribution of B_4C particles. The clusters of B_4C particles in the parent composite were shattered. Some degree of fragmentation of B_4C particles was observed. The hardness of weld zone was higher than that of parent composite. The tensile strength of welded joint was comparable to the strength of the parent composite under the experimental conditions. But FSW reduced the ductility of the joints. The fracture mode changed from ductile to brittle subsequent to FSW.

Acknowledgements

The authors are grateful to the Management and Department of Mechanical Engineering, Coimbatore Institute of Technology, Coimbatore, India. The authors also acknowledge the financial support rendered by the Naval Research Board, Govt. of India. One of the authors, Dr. I. Dinaharan acknowledges the Department of Science and Technology, Govt. of India for providing INSPIRE fellowship. The authors are also thankful to Mr. S. Gopalakrishnan, Mr. S.J. Vijay, Mr. M. Balakrishnan, Mr. R. Sathis Kumar, Mr. G. Sivakumar for their assistance offered to execute the above work.

References

[1] Xiu Z, Yang W, Chen G, Jiang L, Mac K, Wu G. Microstructure and tensile properties of Si_3N4p/2024Al composite fabricated by pressure infiltration method. Mater Des 2012;33:350–5.
[2] Kumar BA, Murugan N. Metallurgical and mechanical characterization of stir cast AA6061-T6-AlNp composite. Mater Des 2012;40:52–8.
[3] Sajjadi SA, Ezatpour HR, Parizi MT. Comparison of microstructure and mechanical properties of A356 aluminum alloy/Al_2O_3 composites fabricated by stir and compo-casting processes. Mater Des 2012;34:106–11.
[4] Dinaharan I, Murugan N. Optimization of friction stir welding process to maximize tensile strength of AA6061/ZrB_2 in situ composite butt joints. Met Mater Int 2012;18:135–42.
[5] Prater T. Solid-state joining of metal matrix composites: a survey of challenges and potential solutions. Mater Manuf Processes 2011;26:636–48.
[6] Storjohann D, Barabash OM, Babu SS, David SA, Sklad PS, Bloom EE. Fusion and friction stir welding of aluminum–metal–matrix composites. Metall Mater Trans A 2005;36:3237–47.

[7] Guo J, Gougeon P, Chen XG. Study on laser welding of AA1100-16 vol.% B_4C metal–matrix composites. Composites Part B 2012;43:2400–8.
[8] Xi-he W, Ji-tai N, Kang GS, Le-jun W, Feng CD. Investigation on TIG welding of SiCp-reinforced aluminum–matrix composite using mixed shielding gas and Al–Si filler. Mater Sci Eng A 2009;499:106–10.
[9] Wang SG, Ji XH, Zhao XQ, Dong NN. Interfacial characteristics of electron beam welding joints of SiCp/Al composites. Mater Sci Technol 2011;27:604.
[10] Cam G. Friction stir welded structural materials: beyond Al-alloys. Int Mater Rev 2011;56:148.
[11] Mishra RS, Ma ZY. Friction stir welding and processing. Mater Sci Eng R 2005;50:1–78.
[12] Nandan R, Debroy T, Bhadeshia HKDH. Recent advances in friction stir welding – process, weldment structure and properties. Prog Mater Sci 2008;53:980–1023.
[13] Threadgill PL, Leonard AJ, Shercliff HR, Withers PJ. Friction stir welding of aluminium alloys. Int Mater Rev 2009;54:49–93.
[14] Chen XG, Da Silva M, Gougeon P, St-Georges L. Microstructure and mechanical properties of friction stir welded AA6063–B_4C metal matrix composites. Mater Sci Eng A 2009;518:174–84.
[15] Vijay SJ, Murugan N. Influence of tool pin profile on the metallurgical and mechanical properties of friction stir welded Al–10 wt.% TiB_2 metal matrix composite. Mater Des 2010;31:3585–9.
[16] Nami H, Adgi H, Sharifitabar M, Shamabadi H. Microstructure and mechanical properties of friction stir welded Al/Mg_2Si metal matrix cast composite. Mater Des 2010;32:976–83.
[17] Gopalakrishnan S, Murugan N. Prediction of tensile strength of friction stir welded aluminum matrix TiC_p particulate reinforced composite. Mater Des 2011;32:462–7.
[18] Guo J, Amira S, Gougeon P, Chen XG. Effect of the surface preparation techniques on the EBSD analysis of a friction stir welded AA1100-B_4C metal matrix composite. Mater Charact 2011;62:865–77.
[19] Bozkurt Y, Uzun H, Salman S. Microstructure and mechanical properties of friction stir welded particulate reinforced AA2124/SiC/25p–T4 composite. J Compos Mater 2011;45:2237–45.
[20] Dinaharan I, Murugan N. Effect of friction stir welding on microstructure, mechanical and wear properties of AA6061/ZrB_2 in situ cast composites. Mater Sci Eng A 2012;543:257–66.
[21] Guo J, Gougeon P, Chen XG. Characterisation of welded joints produced by FSW in AA 1100-B_4C metal matrix composites. Sci Technol Weld Join 2012;17:85–91.
[22] Periyasamy P, Mohan B, Balasubramanian V. Effect of heat input on mechanical and metallurgical properties of friction stir welded AA6061-10% SiCp MMCs. J Mater Eng Perform 2012;21:2417–28.
[23] Wang D, Xiao BL, Wang QZ, Ma ZY. Friction stir welding of SiCp/2009Al composite plate. Mater Des 2013;47:243–7.
[24] Rejil CM, Dinaharan I, Vijay SJ, Murugan N. Microstructure and sliding wear behavior of AA6360/(TiC + B_4C) hybrid surface composite layer synthesized by friction stir processing on aluminum substrate. Mater Sci Eng A 2012;552:336–44.
[25] Kerti I, Toptan F. Microstructural variations in cast B_4C-reinforced aluminium matrix composites (AMCs). Mater Lett 2008;62:1215–8.
[26] Toptan F, Kilicarslan A, Cigdem M, Kerti I. Processing and microstructural characterization of AA1070 and AA 6063 matrix B_4C_P reinforced composites. Mater Des 2010;31:S87–91.
[27] Ceschini L, Boromei I, Minak G, Morri A, Tarterini F. Effect of friction stir welding on microstructure, tensile and fatigue properties of the AA7005/10 vol.%Al_2O_{3p} composite. Compos Sci Technol 2007;67:605–15.
[28] Minak G, Ceschini L, Boromei I, Ponte M. Fatigue properties of friction stir welded particulate reinforced aluminium matrix composites. Int J Fatigue 2009;32:218–26.
[29] Ashok Kumar B, Murugan N. Metallurgical and mechanical characterization of stir cast AA6061-T6-AlNp composite. Mater Des 2012;40:52–8.
[30] Bauri R, Yadav D, Suhas G. Effect of friction stir processing (FSP) on microstructure and properties of Al–TiC in situ composite. Mater Sci Eng A 2011;528:4732–9.
[31] Kennedy AR, Brampton B. The reactive wetting and incorporation of B_4C particles into molten aluminium. Scr Mater 2001;44:1077–82.
[32] Ceschini L, Boromei I, Minak G, Morri A, Tarterini F. Microstructure, tensile and fatigue properties of AA6061/20 vol.%Al_2O_3p friction stir welded joints. Composites Part A 2007;38:1200–10.
[33] Amirizad M, Kokabi AH, Gharacheh MA, Sarrafi R, Shalchi B, Azizieh M. Evaluation of microstructure and mechanical properties in friction stir welded A356 + 15%SiCp cast composite. Mater Lett 2006;60:565–8.